Physics of Fluids

Interaction of wave with multiple wide polynyas

Cite as: Phys. Fluids **31**, 067111 (2019); https://doi.org/10.1063/1.5098877
Submitted: 04 April 2019 . Accepted: 06 June 2019 . Published Online: 27 June 2019

Y. Y. Shi (石玉云), Z. F. Li (李志富), and G. X. Wu (吴国雄)

Interaction of wave with multiple wide polynyas

Cite as: Phys. Fluids 31, 067111 (2019); doi: 10.1063/1.5098877
Submitted: 4 April 2019 • Accepted: 6 June 2019 •
Published Online: 27 June 2019

Y. Y. Shi (石玉云),[1] Z. F. Li (李志富),[2] and G. X. Wu (吴国雄)[2,3,a)]

AFFILIATIONS

[1]College of Shipbuilding Engineering, Harbin Engineering University, Harbin 150001, China
[2]School of Naval Architecture and Ocean Engineering, Jiangsu University of Science and Technology, Zhenjiang 212003, China
[3]Department of Mechanical Engineering, University College London, Torrington Place, London WC1E 7JE, United Kingdom

[a)]**Author to whom correspondence should be addressed:** g.wu@ucl.ac.uk. **Tel.:** +44 20 7679 3870. **Fax:** +44 20 7388 0180.

ABSTRACT

A method based on the wide spacing approximation is applied to the wave scattering problem in multiple polynyas. An ice sheet is modeled as an elastic plate, and fluid flow is described by the velocity potential theory. The solution procedure is constructed based on the assumption that the ice sheet length is much larger than the wavelength. For each polynya, of free surface with an ice sheet on each side, the problem is solved exactly within the framework of the linearized velocity potential theory. This is then matched with the solution from neighboring polynyas at their interfaces below the ice sheet on each side, and only the traveling waves are included in the matching. Numerical results are provided to show that the method is very accurate and highly efficient. Extensive simulations are then carried out to investigate the effects of the ice sheet number, ice sheet length, distribution of ice sheets, as well as polynya width. The features of wave reflection and transmission are analyzed, and the physical mechanism is discussed.

I. INTRODUCTION

The research over the last decades has significantly advanced our understanding of wave physics and the mechanism of its interaction with sea ices. When the wave propagates into a region covered with an ice sheet, there will be wave reflection and transmission. In such a way, the process of wave propagation in icy water is expected to be much more complex than that in open waters. Reviews on this subject have been given by Squire *et al.*[1] and Squire.[2,3] For open water, it is common to consider the ocean surface as infinitely large and treated as a free surface, on which the pressure is assumed to be atmospheric or constant. In an icy water region, one form of ice, an ice sheet, has a horizontal dimension of much larger scale than its vertical dimension. In such a case, the ice sheet could be considered as an elastic plate,[4] and this model has been widely used in the simulations of wave propagation in the polar region. A semi-infinite ice sheet floating on the free-surface was investigated based on the thin plate model[5] and the thick plate model by Fox and Squire,[6] by adopting the matched eigenfunction expansion method. The work was extended by Fox and Squire[7] for wave propagations from open water into a semi-infinite ice sheet covered region obliquely. They showed that beyond a critical incident wave angle, the wave would be totally reflected. For some similar physical problems, an inner product of orthogonality was introduced to solve the unknowns in the eigenfunction expansions, e.g., Sahoo, Yip, and Chwang,[8] in which the ice sheets with various edge conditions were discussed. Meylan and Squire[9] adopted the Green function method due to its flexibility and a much wider range of applications. Other methods have also been used, for instance, the Wiener-Hopf method.[10] Chung and Fox[11] used the method for oblique reflection and transmission of ocean waves into the semi-infinite ice sheet. Other notable work using the Wiener-Hopf method includes those by Balmforth and Craster,[12] and by Tkacheva.[13] Chung and Linton[14] constructed the solution of wave propagating across a polynya between two semi-infinite ice sheets, where the problem was solved with the residue calculus technique. They found that the reflection coefficients could be zero at discrete frequencies. Williams and Squire[15] solved a more general problem of wave interaction with three connected plates of different thicknesses, in which the Wiener-Hopf method and the residue calculus method were both used. When the thickness of the middle one is taken as zero, it becomes a free surface. Thus, polynya can be classified as a special case of this problem. While the thicknesses of two side ice sheets are equal to zero, it becomes an ice floe problem.

Further experimental study on wave interaction with a sea ice floe was conducted by Meylan *et al.*[16]

There has also been work on ice sheets with imperfections, such as cracks. Based on the matched eigenfunction expansions, Barrett and Squire[17] solved the wave propagation through an ice sheet with a crack for finite water depth, where full transmission was observed at a specific period. By adopting the Green function of an infinite homogeneous ice sheet, Squire and Dixon[18] derived an analytical solution for infinite water depth. Following a similar procedure, the work was extended by Squire and Dixon[19] to an ice sheet with multiple cracks, in which the full transmissions occurred at discrete periods. Evans and Porter[20] obtained an analytical solution of the single crack in a series form by dividing the problem into the symmetric and antisymmetric parts, for finite water depth and oblique incident waves. Porter and Evans[21] investigated the wave propagation through multiple cracks, and stopping bands were observed in a semi-infinite array of cracks, where the transmission coefficient was zero. They also obtained the solution for ice sheet with finite length cracks.[22] When there was a body present, Li, Wu, and Ji[23] used the multipole method and obtained solution for a circular cylinder submerged below the ice sheet with a crack. The three dimensional diffraction problem by a circular crack was considered by Li, Wu, and Shi.[24]

A submerged or floating body in a polynya between two semi-infinite ice sheets has also been investigated. Sturova[25] considered a circular cylinder submerged by a polynya. Ren, Wu, and Thomas[26] obtained solution for a rectangular box floating in a polynya between two semi-infinite ice sheets based on a matched eigenfunction expansion. Li, Shi, and Wu[27] considered a more general problem of a two dimensional arbitrarily shaped body based on a hybrid method. Later, a method based on the wide space approximation was adopted for the interaction of waves with a body in a single and wide polynya.[28]

The present work attempts to construct a fast and accurate method for wave ice interaction in multiple polynyas. Based on the wide space approximation, the solution can be constructed from that for a single polynya, which is already available. The merit of the method is that the effort required for solution is minimal as the number of polynyas increases, while the accuracy can be maintained for a high degree. The results may have a wide range of applications in polar engineering. In Sec. II, formulation based on the wide space method is explicitly derived. The numerical validation is first given in Sec. III, which is followed by in-depth investigation on the wave reflection and transmission process through the polynyas. The effects of the ice sheet number and length, polynya width, and distribution of ice sheets are discussed. Conclusions are then drawn in Sec. IV.

II. MATHEMATICAL MODEL AND NUMERICAL PROCEDURES

A. Mathematical model

We consider the wave propagation through $n-1$ polynyas formed by n ice sheets, as sketched in Fig. 1. A Cartesian coordinate system $\vec{x} = (x, z)$ fixed in space is defined with the origin O at the undisturbed mean water surface, x being the horizontal direction and z being vertically upwards. The left and right edges of the jth ice sheet are at x_j^L and x_j^R, respectively. The first and last ice sheets are both semi-infinite or $x_1^L = -\infty$ and $x_n^R = +\infty$, respectively, on the basis that their edges are sufficiently away. The width of the jth polynya is $l_{F,j} = x_{j+1}^L - x_j^R$, $j = 1, \ldots, n-1$. The width of the jth ice sheet is $l_{I,j} = x_j^R - x_j^L$, $j = 1, \ldots, n$, with $l_{I,1}$ and $l_{I,n}$ being infinite. This work is undertaken on the basis that the length of each ice sheet is much larger than the wavelength l, i.e., $l_{I,j} \gg l$. The fluid with density ρ and constant depth H is assumed to be inviscid, incompressible, and homogeneous, and its motion is assumed to be irrotational. Under the assumption that the amplitude of wave motion is small compared to its length, the linearized velocity potential theory can be used to describe the fluid flow. When the motion is sinusoidal in time with radian frequency ω, the total potential can be written as

$$\Phi(x,y,z,t) = \mathrm{Re}[\alpha_0 \phi(x,z) e^{i\omega t}] = \mathrm{Re}\{\alpha_0[\phi_I(x,z) + \phi_D(x,z)] e^{i\omega t}\}, \tag{1}$$

where ϕ_I is the potential due to the incident wave with unit amplitude, ϕ_D is the diffracted potential, and α_0 is the amplitude of the incident wave. Mass conservation requires that the potential ϕ_D satisfies Laplace's equation

$$\nabla^2 \phi_D = 0, \tag{2}$$

throughout the fluid. The combination of the linearized dynamic and kinematic free surface boundary conditions yields

$$-\omega^2 \phi_D + g\frac{\partial \phi_D}{\partial z} = 0, \; (x_j^R < x < x_{j+1}^L, \; j = 1, \ldots, n-1, \; z = 0), \tag{3}$$

in which g is the acceleration due to gravity. Each ice sheet is modeled as a continuous elastic plate with uniform properties, or the density ρ_j, Young's modulus E_j, Poisson's ratio ν_j, thickness h_j, and

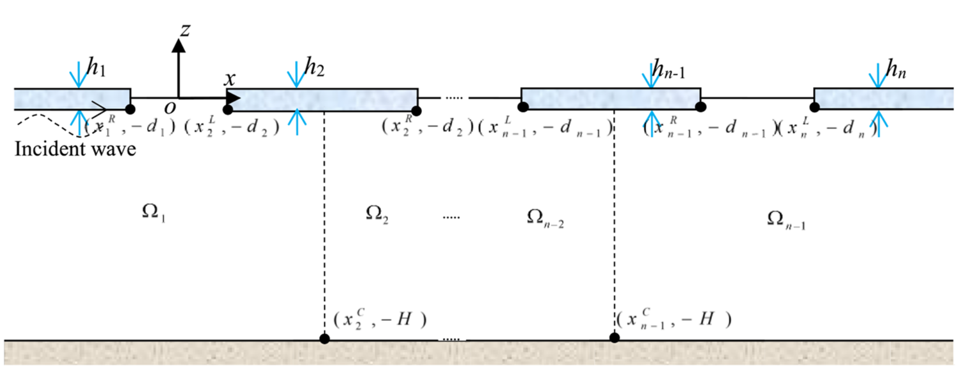

FIG. 1. Coordinate system and sketch of the problem.

draught d_j are all taken to be constant. The boundary condition on the ice sheets can be written as

$$\left(L_j\frac{\partial^4}{\partial x^4} - m_j\omega^2 + \rho g\right)\frac{\partial\phi}{\partial z} - \rho\omega^2\phi = 0,$$
$$(x_j^L \le x \le x_j^R,\quad j = 1,\ldots,n,\quad z = -d_j), \tag{4}$$

where $L_j = Eh_j^3/[12(1-\nu_j^2)]$ and $m_j = h_j\rho_j$ denote, respectively, the effective flexural rigidity of the jth ice sheet and its mass per unit area. Without loss of generality, the two ends of each ice sheet are assumed to be free. Therefore, zero bending moment and shear force, respectively, give

$$\frac{\partial^2}{\partial x^2}\left(\frac{\partial\phi}{\partial z}\right) = 0 \text{ and } \frac{\partial^3}{\partial x^3}\left(\frac{\partial\phi}{\partial z}\right) = 0,$$
$$(x_j^L, -d_j) \text{ or } (x_{j-1}^R, -d_j),\quad j = 2,\ldots,n. \tag{5}$$

On the vertical surface of the ice sheet edge, the impermeable condition yields

$$\frac{\partial\phi}{\partial x} = 0,\quad (x_j^L, -d_j) \text{ or } (x_{j-1}^R, -d_j),\quad -d_j \le z \le 0,\quad j = 2,\ldots,n. \tag{6}$$

On the flat seabed, the boundary condition can be written as

$$\frac{\partial\phi_D}{\partial z} = 0,\ (-\infty < x < +\infty,\quad z = -H). \tag{7}$$

The radiation condition ensures the wave to propagate outwards,

$$\lim_{x\to-\infty}\left(\frac{\partial\phi_D}{\partial x} - \kappa_0^{(1)}\phi_D\right) = 0,\quad \lim_{x\to+\infty}\left(\frac{\partial\phi_D}{\partial x} + \kappa_0^{(n)}\phi_D\right) = 0, \tag{8}$$

where $\kappa_0^{(j)}$ are the purely positive imaginary roots of the dispersion equations

$$-\kappa_0^{(j)}\tan[\kappa_0^{(j)}(H-d_j)] = \frac{\rho\omega^2}{L_j(\kappa_0^{(j)})^4 + \rho g - m_j\omega^2},\quad (j = 1,\ldots,n), \tag{9}$$

below the jth ice sheet. For the problem considered below, when the incoming wave is from $x = \mp\infty$, the corresponding incident potential can be written as

$$\phi_I^L = Ie^{-\kappa_0^{(1)}x}f^{(1)}(z) \text{ and } \phi_I^R = Ie^{\kappa_0^{(n)}x}f^{(n)}(z), \tag{10}$$

where $I = g/\mathrm{i}\omega$, $f^{(j)}(z) = \cos[\kappa_0^{(j)}(z+H)]/\cos[\kappa_0^{(j)}(H-d_j)]$.

B. Solution procedure

For each polynya, we assume that the lengths of the ice sheets on both sides are much larger than its own length. In such a case, the two ice sheets can be approximated as semi-infinite. We take the jth polynya as an example, as sketched in Fig. 2, where the origin O is the center of the polynya. This is effectively a single polynya problem, which has been considered extensively previously, for example, in the work of Ren, Wu, and Thomas.[26] Here, corresponding to the incident wave potentials $\phi_I^L(X,Z)$ from $X = -\infty$ and $\phi_I^R(X,Z)$ from $X = +\infty$ in the form of Eq. (10) with I being taken as unit, we have diffraction potentials $\phi_D^L(X,Z)$ and $\phi_D^R(X,Z)$. In such a case, the combined incident and diffracted wave potentials ψ_L and ψ_R at infinity can be written as

$$\psi_L^{(j)} = (e^{-\kappa_0^{(j)}X} + R_L^{(j)}e^{+\kappa_0^{(j)}X})f^{(j)}(Z) \text{ as } X\to-\infty, \tag{11}$$
$$\psi_L^{(j)} = T_L^{(j)}e^{-\kappa_0^{(j+1)}X}f^{(j+1)}(Z) \text{ as } X\to+\infty, \tag{12}$$
$$\psi_R^{(j)} = T_R^{(j)}e^{+\kappa_0^{(j)}X}f^{(j)}(Z) \text{ as } X\to-\infty, \tag{13}$$
$$\psi_R^{(j)} = (e^{+\kappa_0^{(j+1)}X} + R_R^{(j)}e^{-\kappa_0^{(j+1)}X})f^{(j+1)}(Z) \text{ as } X\to+\infty, \tag{14}$$

where R is the reflection coefficient, T denotes the transmission coefficient, and their subscripts indicate whether the incident wave is from the left hand side or from the right.

When the single polynya in Fig. 2 is put back into the original problem in Fig. 1, the incident waves are originated from the two neighboring polynyas. Their amplitudes ε and γ are generally unknown. The velocity potential $\phi^{(j)}$ in Ω_j may be written as

$$\phi^{(j)}(x,z) = \varepsilon^{(j)}\psi_L^{(j)}(x-x_j,z) + \gamma^{(j)}\psi_R^{(j)}(x-x_j,z),\quad (j = 1,\ldots,n-1), \tag{15}$$

where $x_j = (x_j^R + x_{j+1}^L)/2$, which is used due to the fact that Eqs. (11)–(14) are based on that the origin of XZ is at the center of the polynya. At the interface of Ω_j and Ω_{j+1}, or $x = x_{j+1}^C$ shown in Fig. 1, pressure and velocity continuity conditions yield

$$\phi^{(j)}(x_{j+1}^C,z) = \phi^{(j+1)}(x_{j+1}^C,z),\quad \frac{\partial\phi^{(j)}(x_{j+1}^C,z)}{\partial x} = \frac{\partial\phi^{(j+1)}(x_{j+1}^C,z)}{\partial x},$$
$$(j = 1,\ldots,n-2). \tag{16}$$

We notice that x_{j+1}^C may be treated as $X\to\infty$ for Ω_j and as $X\to-\infty$ for Ω_{j+1}. This allows Eqs. (12) and (14) to be substituted into the left hand side of Eq. (16) and Eqs. (11) and (13) into the right hand side.

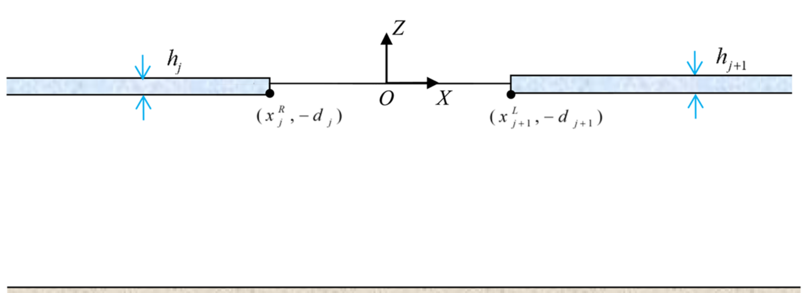

FIG. 2. Sketch of a single polynya.

Together with Eq. (15), we have

$$\varepsilon^{(j)}T_L^{(j)}e^{-\kappa_0^{(j+1)}\left(x_{j+1}^C-x_j\right)}+\gamma^{(j)}\left(e^{+\kappa_0^{(j+1)}\left(x_{j+1}^C-x_j\right)}+R_R^{(j)}e^{-\kappa_0^{(j+1)}\left(x_{j+1}^C-x_j\right)}\right)$$
$$=\varepsilon^{(j+1)}\left(e^{-\kappa_0^{(j+1)}\left(x_{j+1}^C-x_{j+1}\right)}+R_L^{(j+1)}e^{+\kappa_0^{(j+1)}\left(x_{j+1}^C-x_{j+1}\right)}\right)$$
$$+\gamma^{(j+1)}T_R^{(j+1)}e^{+\kappa_0^{(j+1)}\left(x_{j+1}^C-x_{j+1}\right)}, \tag{17}$$

$$-\varepsilon^{(j)}T_L^{(j)}e^{-\kappa_0^{(j+1)}\left(x_{j+1}^C-x_j\right)}+\gamma^{(j)}\left(e^{+\kappa_0^{(j+1)}\left(x_{j+1}^C-x_j\right)}-R_R^{(j)}e^{-\kappa_0^{(j+1)}\left(x_{j+1}^C-x_j\right)}\right)$$
$$=\varepsilon^{(j+1)}\left(-e^{-\kappa_0^{(j+1)}\left(x_{j+1}^C-x_{j+1}\right)}+R_L^{(j+1)}e^{+\kappa_0^{(j+1)}\left(x_{j+1}^C-x_{j+1}\right)}\right)$$
$$+\gamma^{(j+1)}T_R^{(j+1)}e^{+\kappa_0^{(j+1)}\left(x_{j+1}^C-x_{j+1}\right)} \tag{18}$$

for $j = 1, \ldots, n-2$. Subtraction and summation of Eqs. (17) and (18), respectively, yield

$$T_L^{(j)}\varepsilon^{(j)}+R_R^{(j)}\gamma^{(j)}-S^{(j+1)}\varepsilon^{(j+1)}=0, \tag{19}$$

$$-S^{(j+1)}\gamma^{(j)}+R_L^{(j+1)}\varepsilon^{(j+1)}+T_R^{(j+1)}\gamma^{(j+1)}=0, \tag{20}$$

where

$$S^{(j+1)}=e^{\kappa_0^{(j+1)}(x_{j+1}-x_j)}=e^{\kappa_0^{(j+1)}\left[(l_{F,j}+l_{F,j+1})/2+l_{I,j+1}\right]}. \tag{21}$$

If we assume that the wave in Fig. 1 is from $x = -\infty$, then $\varepsilon^{(1)} = 1$ and $\gamma^{(n-1)} = 0$. Since $R_L^{(j)}$, $R_R^{(j)}$, $T_L^{(j)}$, and $T_R^{(j)}$ can be obtained from the solution of a single polynya,[26] Eqs. (19) and (20) form $(2n-4)$ linear algebraic equations with $(2n-4)$ unknown coefficients. In matrix form, these equations can be written as

$$QX = D, \tag{22}$$

where

$$Q=\begin{bmatrix} b_1 & c_1 & & & \\ a_2 & b_2 & c_2 & & \\ & a_3 & \ddots & \ddots & \\ & & \ddots & \ddots & c_{2n-5} \\ & & & a_{2n-4} & b_{2n-4}\end{bmatrix}. \tag{23}$$

Q is a tridiagonal matrix, where

$$\begin{cases} a_{2j}=-S^{(j+1)}, j=1,\ldots,n-2 \\ a_{2j+1}=T_L^{(j+1)}, j=1,\ldots,n-3 \end{cases},\quad \begin{cases} b_{2j-1}=R_R^{(j)}, j=1,\ldots,n-2 \\ b_{2j}=R_L^{(j+1)}, j=1,\ldots,n-2 \end{cases},\quad \begin{cases} c_{2j-1}=-S^{(j+1)}, j=1,\ldots,n-2 \\ c_{2j}=T_R^{(j+1)},, j=1,\ldots,n-3 \end{cases}, \tag{24}$$

and

$$X=\begin{bmatrix}\gamma^{(1)}\\ \varepsilon^{(2)}\\ \gamma^{(2)}\\ \vdots\\ \varepsilon^{(n-1)}\end{bmatrix}, D=\begin{bmatrix} d_1\\ d_2\\ \vdots\\ \vdots\\ d_{2n-4}\end{bmatrix}, \tag{25}$$

with

$$d_j=\begin{cases}-T_L^{(j)}, j=1\\ 0, j=2,\ldots,2n-4\end{cases}. \tag{26}$$

Here, $R_L^{(j)}$, $R_R^{(j)}$, $T_L^{(j)}$, and $T_R^{(j)}$ are obtained from the exact solution of each subdomain in Fig. 2 and then they are subsequently used in the problem in Fig. 1. The fact is that the problem in Fig. 2 can also be obtained using the wide spacing approximation when the width of the polynya is much larger than the wavelength. In fact, Li *et al.*[28] have found that the approximation provides very accurate results over an almost entire wavelength range. This will be further discussed when results are provided.

For the problem in Fig. 1, for wave from $x = -\infty$, we have the asymptotic form of the velocity potential at infinity

$$\phi(x,z)=\begin{cases} e^{-\kappa_0^{(1)}(x-x_1)}+\mathcal{R}e^{\kappa_0^{(1)}(x-x_1)}\varphi^{(1)}(z), & x\to-\infty\\ \mathcal{T}e^{-\kappa_0^{(n)}(x-x_{n-1})}\varphi^{(n)}(z), & x\to+\infty\end{cases}, \tag{27}$$

where $\mathcal{R}$ and $\mathcal{T}$ are overall reflection and transmission coefficients, respectively. Based on Eqs. (11)–(14) and (15), we have

$$\mathcal{R}=R_L^{(1)}+\gamma^{(1)}T_R^{(1)},\quad \mathcal{T}=\varepsilon^{(n-1)}T_L^{(n-1)}. \tag{28}$$

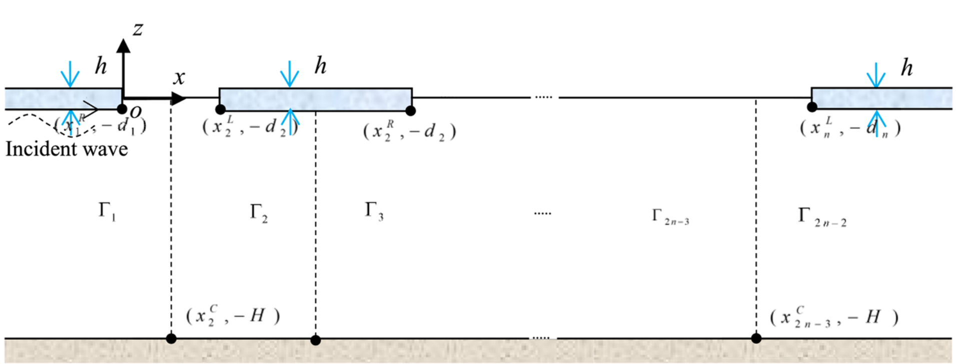

FIG. 3. Sketch of alternative domain decomposition.

Alternative domain decomposition for approximation can also be adopted, as shown in Fig. 3. In each subpolynya, the domain is divided into two parts. In one part, the wave is from a semi-infinite ice sheet to the semi-infinite free surface, while in the other part it is the other way round. The problem in Fig. 1 is then divided into $2n-2$ subdomains. For the $(2j-1)$-th subdomain, we have ice sheet to free surface, and the potential can be written as

$$\psi_L^{(2j-1)} = (e^{-\kappa_0^{(j)}X} + R_L^{(2j-1)}e^{+\kappa_0^{(j)}X})f^{(j)}(Z) \text{ as } X \to -\infty, \tag{29}$$

$$\psi_L^{(2j-1)} = T_L^{(2j-1)}e^{-\lambda_0 X}g(Z) \text{ as } X \to +\infty, \tag{30}$$

$$\psi_R^{(2j-1)} = T_R^{(2j-1)}e^{+\kappa_0^{(j)}X}f^{(j)}(Z) \text{ as } X \to -\infty, \tag{31}$$

$$\psi_R^{(2j-1)} = (e^{+\lambda_0 X} + R_R^{(2j-1)}e^{-\lambda_0 X})g(Z) \text{ as } X \to +\infty, \tag{32}$$

where $g(Z) = \cos[\lambda_0(z+H)]/\cos[\lambda_0(H)]$, $\omega^2 = \lambda_0 g\tanh\lambda_0 H$, and $X = 0$ is at the edge of the ice sheet. It should be noted here that $R_L^{(j)}$, $T_L^{(j)}$, $R_R^{(j)}$, and $T_R^{(j)}$ are obtained from the case of the wave from a semi-infinite ice sheet to semi-infinite free surface. Similarly, for the $(2j)$-th subdomain, we have

$$\psi_L^{(2j)} = (e^{-\lambda_0 X} + R_L^{(2j)}e^{+\lambda_0 X})g(Z) \text{ as } X \to -\infty, \tag{33}$$

$$\psi_L^{(2j)} = T_L^{(2j)}e^{-\kappa_0^{(j+1)}X}f^{(j+1)}(Z) \text{ as } X \to +\infty, \tag{34}$$

$$\psi_R^{(2j)} = T_R^{(2j)}e^{+\lambda_0 X}g(Z) \text{ as } X \to -\infty, \tag{35}$$

$$\psi_R^{(2j)} = (e^{+\kappa_0^{(j+1)}X} + R_R^{(2j)}e^{-\kappa_0^{(j+1)}X})f^{(j+1)}(Z) \text{ as } X \to +\infty. \tag{36}$$

Thus, the velocity potential $\phi^{(2j-1)}$, $\phi^{(2j)}$ in Γ_{2j-1} and Γ_{2j} may be written as

$$\begin{cases} \phi^{(2j-1)}(x,z) = \varepsilon^{(2j-1)}\psi_L^{(2j-1)}(x-x_{2j-1},z) + \gamma^{(2j-1)}\psi_R^{(2j-1)}(x-x_{2j-1},z) \\ \phi^{(2j)}(x,z) = \varepsilon^{(2j)}\psi_L^{(2j)}(x-x_{2j},z) + \gamma^{(2j)}\psi_R^{(2j)}(x-x_{2j},z) \end{cases}, \tag{37}$$

in which $x_{2j-1} = x_j^R$ and $x_{2j} = x_j^L$.

The interface of Γ_{2j-1} and Γ_{2j} is below the free surface. The pressure and velocity continuity conditions yield

$$\phi^{(2j-1)}(x_{2j}^C,z) = \phi^{(2j)}(x_{2j}^C,z), \quad \frac{\partial\phi^{(2j-1)}(x_{2j}^C,z)}{\partial x} = \frac{\partial\phi^{(2j)}(x_{2j}^C,z)}{\partial x}. \tag{38}$$

This leads to

$$T_L^{(2j-1)}\varepsilon^{(2j-1)} + R_R^{(2j-1)}\gamma^{(2j-1)} - S^{(2j)}\varepsilon^{(2j)} = 0, \tag{39}$$

$$-S^{(2j)}\gamma^{(2j-1)} + R_L^{(2j)}\varepsilon^{(2j)} + T_R^{(2j)}\gamma^{(2j)} = 0, \tag{40}$$

where

$$S^{(2j)} = e^{\lambda_0(x_{2j}-x_{2j-1})} = e^{\lambda_0 l_{F,j+1}}. \tag{41}$$

The interface of Γ_{2j} and Γ_{2j+1} is below the ice sheet. Similar to (39), it is straightforward to have

$$T_L^{(2j)}\varepsilon^{(2j)} + R_R^{(2j)}\gamma^{(2j)} - S^{(2j+1)}\varepsilon^{(2j+1)} = 0, \tag{42}$$

$$-S^{(2j+1)}\gamma^{(2j)} + R_L^{(2j+1)}\varepsilon^{(2j+1)} + T_R^{(2j+1)}\gamma^{(2j+1)} = 0, \tag{43}$$

where

$$S^{2j+1} = e^{\kappa_0^{(j+1)}(x_{2j+1}-x_{2j})} = e^{\kappa_0^{(j+1)}l_{I,j+1}}. \tag{44}$$

Thus, for a system of n ice sheets with $n-1$ polynyas, it will create $2n-2$ subdomains with $2n-3$ interfaces. This will generate $4n-6$ linear algebraic equations with $4n-6$ unknowns. It should be noted that the coefficient matrix is also a tridiagonal one, similar to that in Eq. (23), with Eq. (24) being replaced by

$$\begin{cases} a_{2j} = -S^{(j+1)}, j = 1,\ldots,2n-3 \\ a_{2j+1} = T_L^{(j+1)}, j = 1,\ldots,2n-4 \end{cases} \quad \begin{cases} b_{2j-1} = R_R^{(j)}, j = 1,\ldots,2n-3 \\ b_{2j} = R_L^{(j+1)}, j = 1,\ldots,2n-3 \end{cases}, \quad \begin{cases} c_{2j-1} = -S^{(j+1)}, j = 1,\ldots,2n-3 \\ c_{2j} = T_R^{(j+1)},, j = 1,\ldots,2n-4 \end{cases}, \tag{45}$$

and correspondingly

$$d_j = \begin{cases} -T_L^{(j)}, & j = 1 \\ 0, & j = 2,\ldots,4n-6 \end{cases}. \tag{46}$$

III. NUMERICAL RESULTS

For the numerical results to be presented in this section, the typical physical parameters of the ice sheet together with water depth are chosen as

$$E = 5 \text{ Gpa}, \; \upsilon = 0.3, \; \rho_j = 922.5 \text{ kg m}^{-3}, \; \rho = 1025 \text{ kg m}^{-3}, \; H = 100 \text{ m}. \tag{47}$$

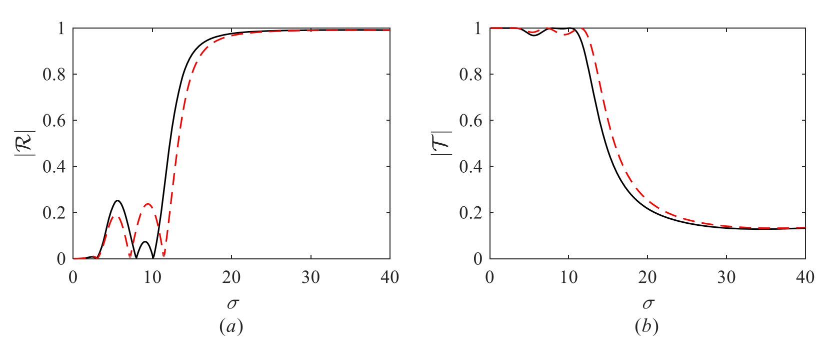

FIG. 4. The modulus of reflection $\mathcal{R}$ and transmission $\mathcal{T}$ coefficients of an ice sheet with two cracks. (a) $|\mathcal{R}|$ and (b) $|\mathcal{T}|$. Solid line: exact solution;[29] dashed line: present result ($n = 3$, $h_j = h = 0.01$, $m_j = m = 0.9$, $L_j = L = 45\,536$, $d_j = d = 0$, $j = 1,2,3$, $l_{I,2} = 0.5$).

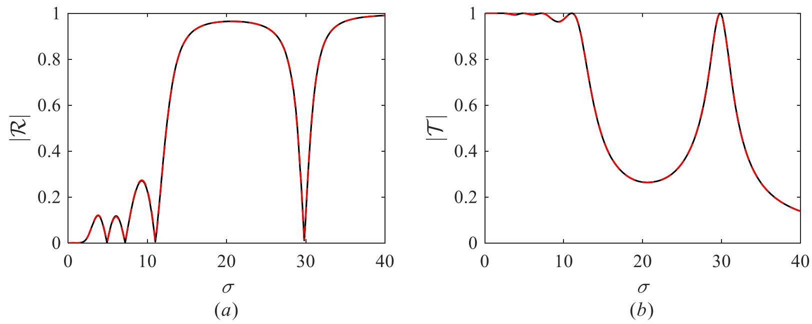

FIG. 5. The modulus of reflection $\mathcal{R}$ and transmission $\mathcal{T}$ coefficients of an ice sheet with two cracks. (a) $|\mathcal{R}|$ and (b) $|\mathcal{T}|$. Solid line: exact solution;[29] dashed line: present result ($n = 3$, $h_j = h = 0.01$, $m_j = m = 0.9$, $L_j = L = 45\,536$, $d_j = d = 0$, $j = 1,2,3$, $l_{I,2} = 1$).

The numerical results will be presented in the nondimensionalized form, with basic parameters chosen as water depth H, water density ρ, and acceleration due to gravity g. The exact solution for the problem of a single polynya in Fig. 2 is obtained based on the procedure in the work of Ren, Wu, and Thomas.[26] The results are then used in Eqs. (19) and (20) for the multiple polynya problem.

Unless it is specified, the results below are obtained from a solution based on a single polynya in Fig. 2 as a subdomain. Results

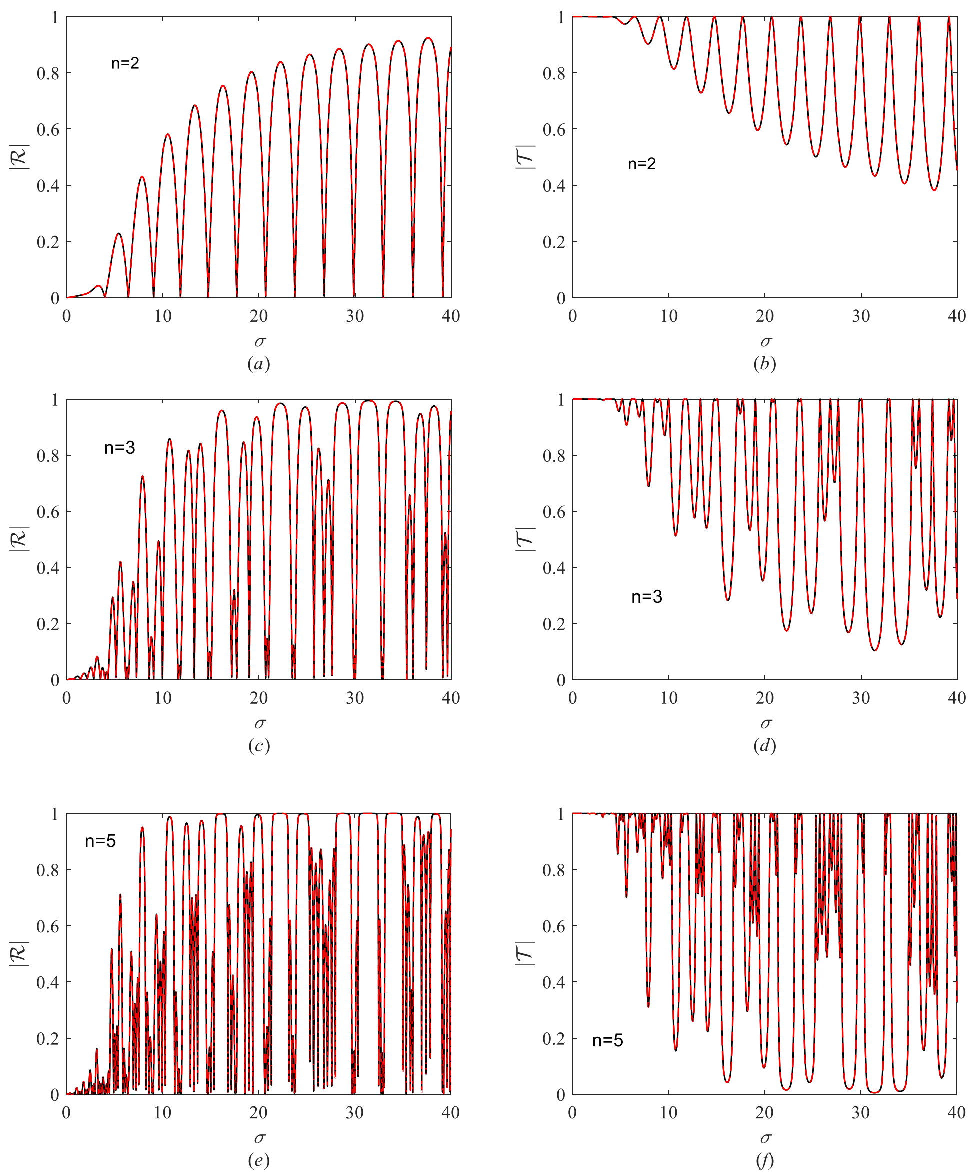

FIG. 6. The modulus of reflection $\mathcal{R}$ and transmission $\mathcal{T}$ coefficients against σ. (a) $|\mathcal{R}|$ for $n = 2$; (b) $|\mathcal{T}|$ for $n = 2$; (c) $|\mathcal{R}|$ for $n = 3$; (d) $|\mathcal{T}|$ for $n = 3$; (e) $|\mathcal{R}|$ for $n = 5$; (f) $|\mathcal{T}|$ for $n = 5$. Solid line: solution from ice-water-ice as a subdomain; dashed line: solution from ice-water or water-ice as a subdomain ($h_j = h = 0.01$, $m_j = m = 0.9$, $L_j = L = 45\,536$, $d_j = d = 0$, $l_{I,j} = l_I = 4.0$, $j = 1, \ldots, n$, $l_{F,j} = l_F = 1.0$, $j = 1, \ldots, n-1$).

from other approximations are presented in some cases, especially for comparison and validation.

A. Verification of the methodology and solution procedure

As demonstrated by Li, Wu, and Ji,[29] when the width of a polynya tends to zero, the result tends to that of a crack. The exact solution for wave reflection and transmission by cracks has been obtained in the work of Li, Wu, and Ji,[29] where a Green function satisfying all the boundary conditions including those at cracks was first derived and then used for obtaining the solution explicitly. To carry out the comparison, we take $l_{F,j} = 0$, $j = 1, \ldots, n-1$ and consider an example of $n = 3$, with $h_j = h = 0.01$, $m_j = m = 0.9$, $L_j = L = 45\,536$, $d_j = d = 0$, $j = 1, 2, 3$. The nondimensional length of the middle ice sheet, or $l_{I,2}$, is taken as 0.5, 1.0. The reflection and transmission coefficients defined in Eq. (27) are, respectively, shown in Figs. 4(a) and 5(a) and Figs. 4(b) and 5(b), against nondimensional frequency σ. For a smaller $l_{I,2}$ in Fig. 4, the present results are close to the exact solution, but some visible discrepancy exists. This discrepancy is not entirely unexpected, as the present method is based on the assumption that the length of the ice sheet between the two polynyas (or cracks) should be sufficiently long. For a larger $l_{I,2}$ in Fig. 5, the discrepancy observed in Fig. 4 disappears. $|\mathcal{R}|$ and $|\mathcal{T}|$ obtained from the present approximate method are in excellent agreement with those from the exact solution.[29] This verifies the present approximate method and solution procedure.

B. Solution for $n-1$ identical subdomains

We first consider the case in which the ice sheets have the same physical properties and length, and polynyas have the same width, $m_j = 0.9$, $L_j = 45\,536$, $l_{F,j} = 1.0$, $l_{I,j} = 4.0$, $j = 1, 2, \ldots, n$. The lengths of the first and the last ice sheets are obviously infinite. Even when n is small, some trend is already forming. In Figs. 6(a)–6(f), results for $n = 2$, $n = 3$, and $n = 5$, are, respectively, provided. It can be seen that, different from an ice-water or water-ice system,[5] the reflection and transmission coefficients of polynyas (single and multiple one) are very oscillatory against the nondimensional wave frequency. The results from multiple polynyas ($n > 2$) become more complex, and there are some local spikes within the calculated nondimensional frequency range due to the mutual interactions between wave

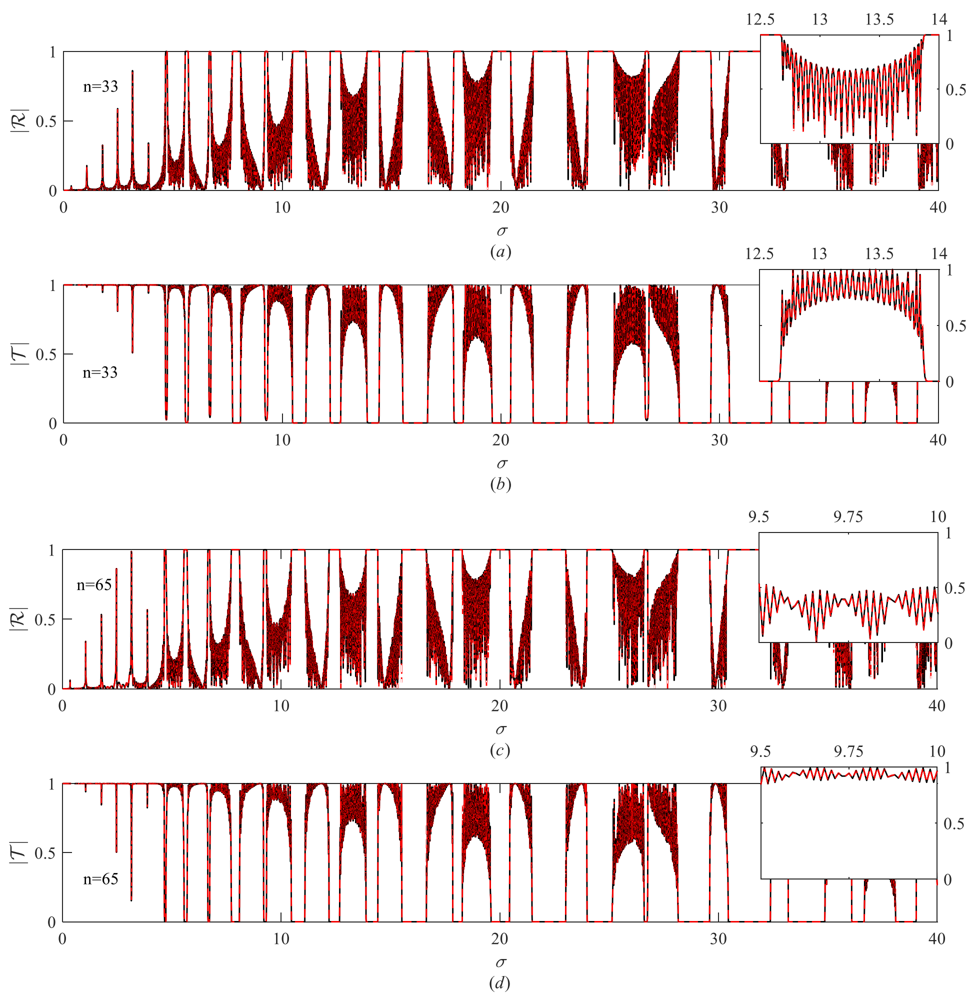

FIG. 7. The modulus of reflection $\mathcal{R}$ and transmission $\mathcal{T}$ coefficients against σ. (a) $|\mathcal{R}|$ for $n = 33$; (b) $|\mathcal{T}|$ for $n = 33$; (c) $|\mathcal{R}|$ for $n = 65$; (d) $|\mathcal{T}|$ for $n = 65$. Solid line: solution for ice-water-ice as a subdomain; dashed line: solution for ice-water or water-ice as a subdomain ($h_j = h = 0.01$, $m_j = m = 0.9$, $L_j = L = 45\,536$, $d_j = d = 0$, $l_{I,j} = l_I = 4.0$, $j = 1, \ldots, n$, $l_{F,j} = l_F = 1.0$, $j = 1, \ldots, n-1$).

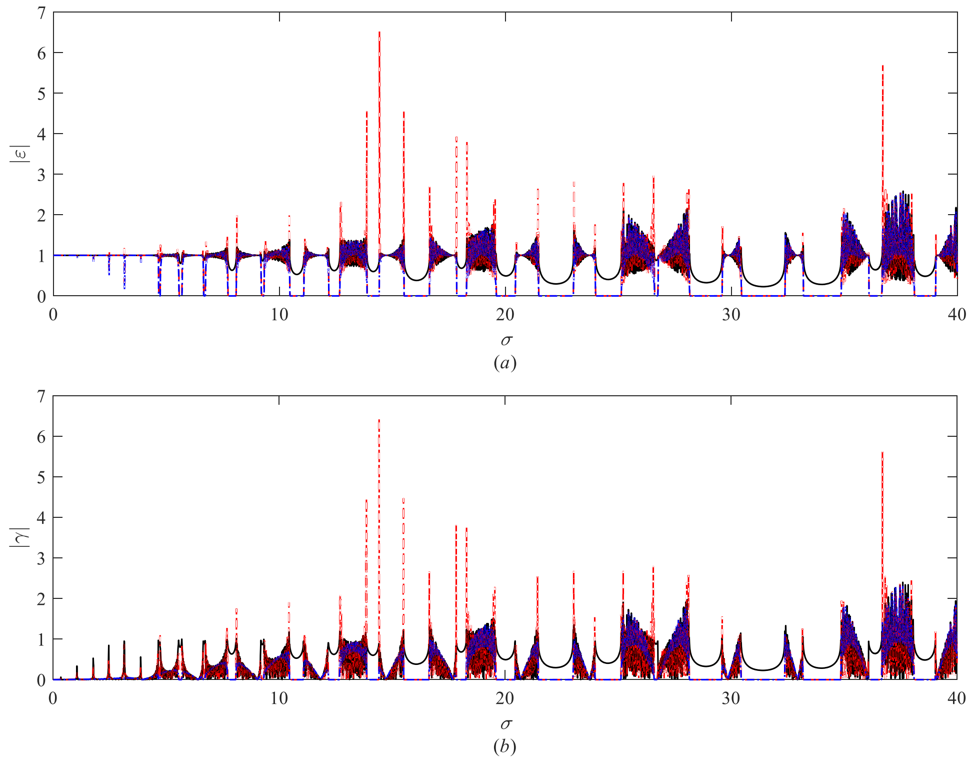

FIG. 8. The modulus of wave amplitudes in polynyas. (a) $|\varepsilon|^{(j)}$ and (b) $|\gamma|^{(j)}$. In (a), solid line: j = 2; dashed line: j = 32; dashed-dotted line: j = 64. In (b), solid line: j = 1; dashed line: j = 31; dashed-dotted line: j = 63 (n = 65, $h_j = h$ = 0.01, $m_j = m$ = 0.9, $L_j = L$ = 45 536, $d_j = d$ = 0, $l_{I,j} = l_I$ = 4.0, j = 1, . . ., n, $l_{F,j} = l_F$ = 1.0, j = 1, . . ., n − 1).

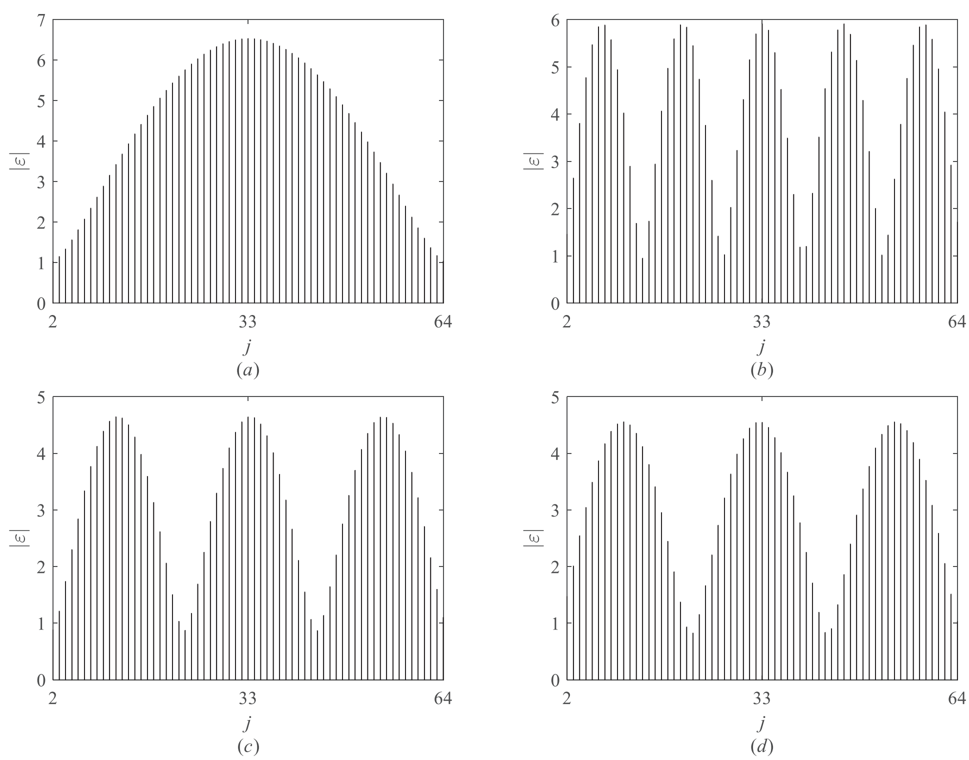

FIG. 9. Variation of coefficient $|\varepsilon|^{(j)}$ with j. (a) σ = 14.43; (b) σ = 36.7; (c) σ = 13.87; (d) σ = 15.51 (n = 65, $h_j = h$ = 0.01, $m_j = m$ = 0.9, $L_j = L$ = 45 536, $d_j = d$ = 0, $l_{I,j} = l_I$ = 4.0, j = 1, . . ., n, $l_{F,j} = l_F$ = 1.0, j = 1, . . ., n−1).

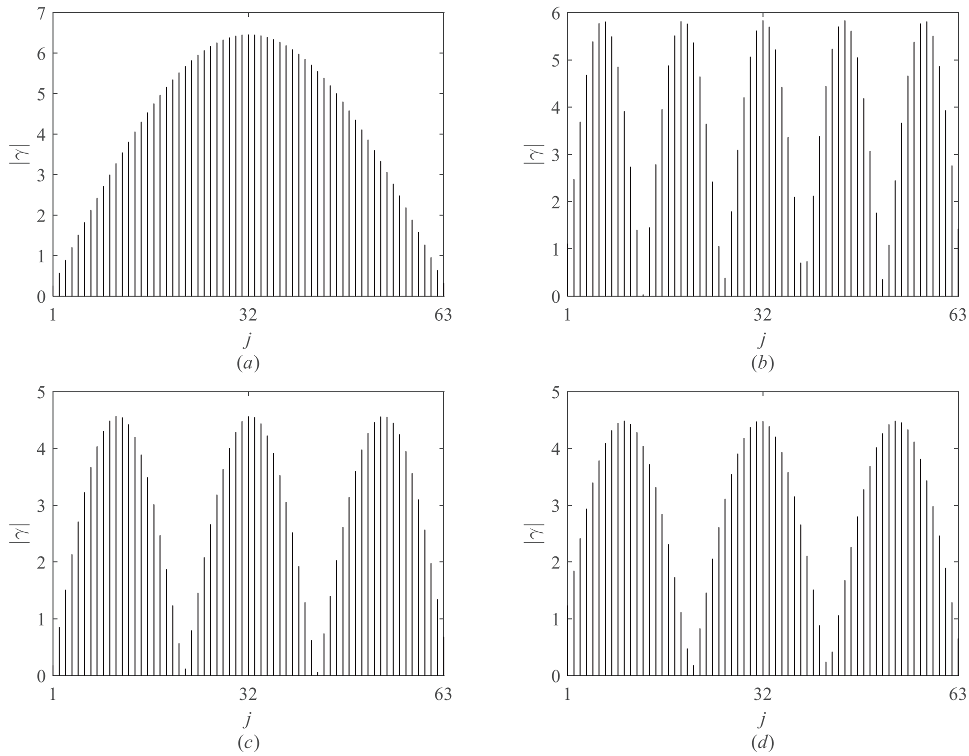

FIG. 10. Variation of coefficient $|\gamma|^{(j)}$ with j. (a) σ = 14.43; (b) σ = 36.7; (c) σ = 13.87; (d) σ = 15.51 (n = 65, h_j = h = 0.01, m_j = m = 0.9, L_j = L = 45 536, d_j = d = 0, $l_{I,j}$ = l_I = 4.0, j = 1, . . ., n, $l_{F,j}$ = l_F = 1.0, j = 1, . . ., n−1).

reflections and transmissions from multiple polynyas. To investigate whether these spikes are due to numerical error, calculations are also undertaken based on the subdomain of ice-water or water-ice in Fig. 3. The obtained results are also plotted in Fig. 6. It can be seen that the curves from different subdomains coincide very well with each other, which confirms the observed behavior.

It has been shown in the work of Li, Shi, and Wu[28] that for a single polynya, or n = 2, at certain discrete frequencies, there is no wave reflection or R = 0. In Fig. 6, it can be seen that at the same frequency $\mathcal{R}$ = 0 at n = 3 and n = 5. Further calculations for cases of large n are undertaken, and the results for n = 33 and n = 65 are plotted in Fig. 7. It is interesting to see that these discrete frequencies at which $\mathcal{R}$ = 0 are not affected by n. For a single polynya, the reason for zero reflection was explained explicitly in the work of Li, Shi, and Wu.[28] Here, when the subdomain is identical and zero reflection occurs, we have $R_R^{(j)} = R_L^{(j)} = 0$ and $\left|T_R^{(j)}\right| = \left|T_L^{(j)}\right| = 1, j = 1, 2, \ldots, n - 1$). From Eqs. (19) and (20), we have $\left|\varepsilon^{(j)}\right| = 1$ and $\gamma^{(j)} = 0$. From Eq. (28), then $|\mathcal{R}| = 0$ and $|\mathcal{T}| = 1$, which is independent of n. Physically, when the incident wave passes through the first polynya and is fully transmitted without any reflection, it will enter the second polynya in the exactly same form, which will be fully transmitted and not be reflected. This will continue no matter how many polynyas there are.

It can be observed in Fig. 7 that at large n, when $R \neq 0$, or when the wave is reflected, $|\mathcal{R}|$ is very close to 1 within some discrete bands, or the wave is fully reflected in these bands. A similar phenomenon has also been observed in equally spaced multiple cracks.[29] In fact, in the case of infinite number of cracks, it has been shown[21] that $\mathcal{T}$ = 0 at an infinite number of discrete bands and the band has

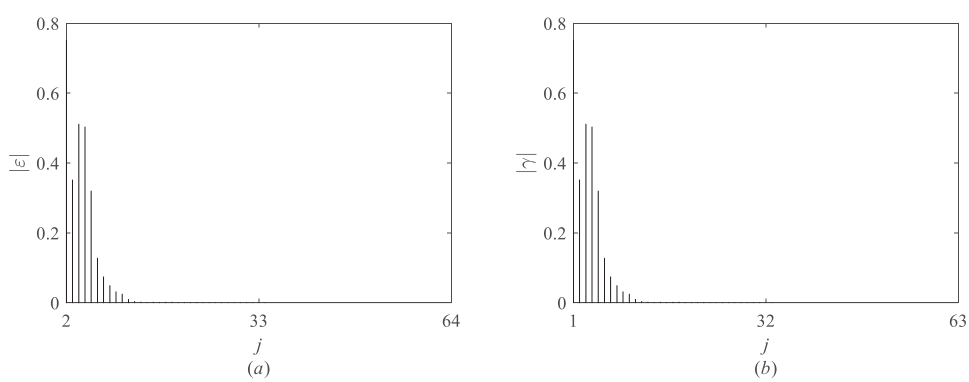

FIG. 11. Variation of coefficient against j. (a) $|\varepsilon|^{(j)}$ and (b) $|\gamma|^{(j)}$ (n = 65, σ = 16, h_j = h = 0.01, m_j = m = 0.9, L_j = L = 45 536, d_j = d = 0, $l_{I,j}$ = l_I = 4.0, j = 1, . . ., n, $l_{F,j}$ = l_F = 1.0, j = 1, . . ., n−1).

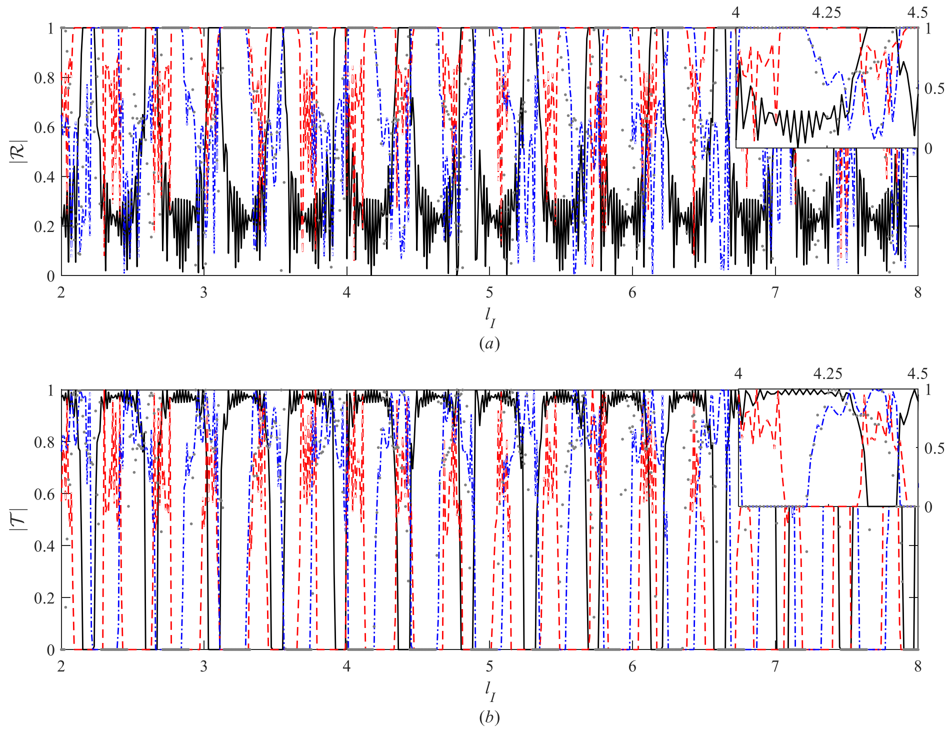

FIG. 12. The modulus of reflection $\mathcal{R}$ and transmission $\mathcal{T}$ coefficients against l_I. (a) $|\mathcal{R}|$ and (b) $|\mathcal{T}|$. Solid line: σ = 14.43; dashed line: σ = 36.7; dashed-dotted line: σ = 13.87; dotted line: σ = 15.51 (n = 65, $h_j = h$ = 0.01, $m_j = m$ = 0.9, $L_j = L$ = 45 536, $d_j = d = 0$, j = 1, . . ., n, $l_{F,j} = l_F$ = 1.0, j = 1, . . ., n−1).

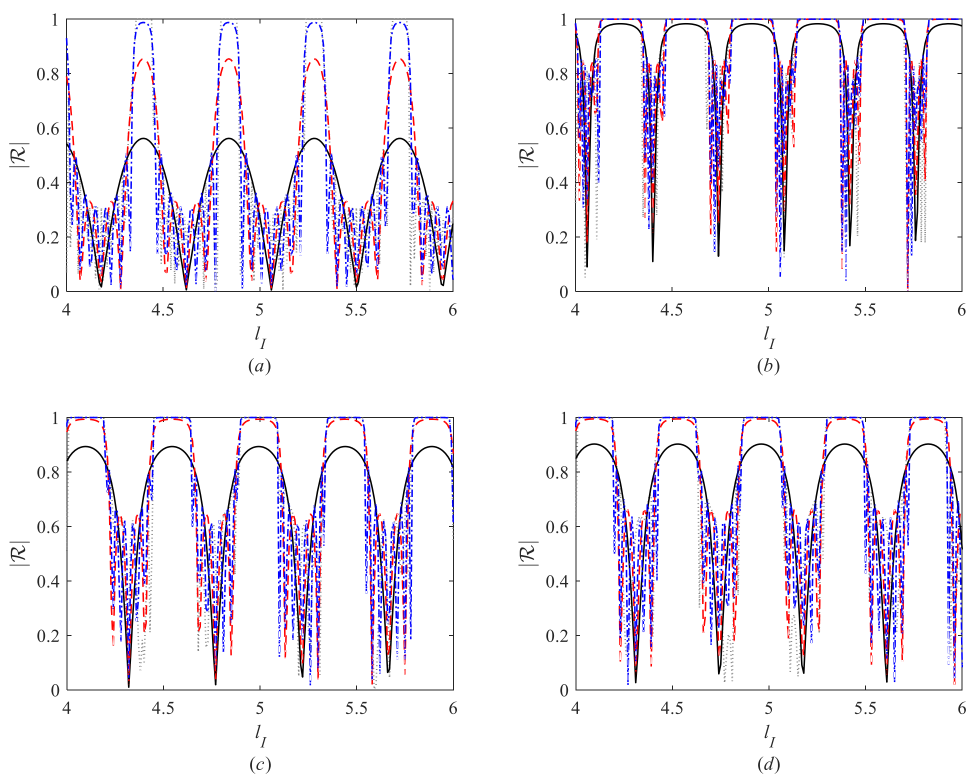

FIG. 13. The modulus of reflection coefficient $\mathcal{R}$ against l_I. (a) σ = 14.43; (b) σ = 36.7; (c) σ = 13.87; (d): σ = 15.51. Solid line: n = 3; dashed line: n = 5; dashed-dotted line: n = 9; dotted line: n = 65 ($h_j = h$ = 0.01, $m_j = m$ = 0.9, $L_j = L$ = 45 536, $d_j = d$ = 0, j = 1, . . ., n, $l_{F,j} = l_F$ = 1.0, j = 1, . . ., n − 1).

been named as the stopping band. To explain the phenomenon, we can solve the problem successively by increasing n, and corresponding reflection and transmissions are denoted by $\mathcal{R}_L{}^{(n)}$ and $\mathcal{T}_L^{(n)}$, respectively. Assume the problem at $n-1$ has been solved. Another polynya is then added to the problem. The problem of n ice sheets is divided into two subdomains: one with $n-1$ ice sheets and the other with two ice sheets. Through imposing the continuity condition at their interface, as done previously, we have

$$\gamma^{(1)} = \frac{\mathcal{T}_L^{(n-1)} R_L^{(2)}}{[S^{(n)}]^2 - \mathcal{R}_R^{(n-1)} R_L^{(2)}}, \quad \varepsilon^{(2)} = \frac{\mathcal{T}_L^{(n-1)} [S^{(n)}]^2}{[S^{(n)}]^2 - \mathcal{R}_R^{(n-1)} R_L^{(2)}}. \tag{48}$$

Substituting Eq. (48) into Eq. (28), we have

$$\begin{aligned} \mathcal{R}_L{}^{(n)} &= \mathcal{R}_L^{(n-1)} + \gamma^{(1)} \mathcal{T}_R^{(n-1)} = \mathcal{R}_L^{(n-1)} + \frac{\mathcal{T}_L^{(n-1)} \mathcal{T}_R^{(n-1)} R_L^{(2)}}{[S^{(n)}]^2 - \mathcal{R}_R^{(n-1)} R_L^{(2)}}, \\ \mathcal{T}_L{}^{(n)} &= \varepsilon_n^{(2)} T_L^{(2)} = \alpha_n \alpha_{n-1} \alpha_{n-2} \ldots \alpha_3 \left[T_L^{(2)} \right]^{n-1}, \end{aligned} \tag{49}$$

in which

$$\alpha_n = \frac{[S^{(n)}]^2}{[S^{(n)}]^2 - \mathcal{R}_R^{(n-1)} R_L^{(2)}}. \tag{50}$$

Equation (49) shows that when $R_L{}^{(2)} = 0$, or when there is no reflection from a single polynya, then $\mathcal{R}_L{}^{(n)} = 0$ and $\left|\mathcal{T}_L^{(n)}\right| = 1$. This is consistent with the previous analysis. In the region of relatively small $T_L{}^{(2)}$, noticing $\left|T_L^{(2)}\right| < 1$, $\left|T_L^{(2)}\right|^{n-1}$ will tend to zero as n increases, leading to a stopping band. However, in other regions, it will depend on the relative magnitudes of α_n and $T_L{}^{(2)}$, leading to a highly oscillatory behavior of $\mathcal{T}_L^{(n)}$. This is reflected in Fig. 7 and is consistent with Conclusion 5 of Li, Wu, and Ji.[29]

For each polynya j, the base solution ψ is the same and the difference is in $\varepsilon^{(j)}$ and in $\gamma^{(j)}$. Physically, $\varepsilon^{(j)}$ refers to the wave from the left side, and $\gamma^{(j)}$ denotes the wave coming from the right side, which are the magnitudes of the waves propagating in opposite directions in each subpolynya. Figures 8(a) and 8(b), respectively, show the coefficients $\left|\varepsilon^{(j)}\right|$, $j = 2$, 32, and 64 and $\left|\gamma^{(j)}\right|$, $j = 1$, 31, and 63 for the

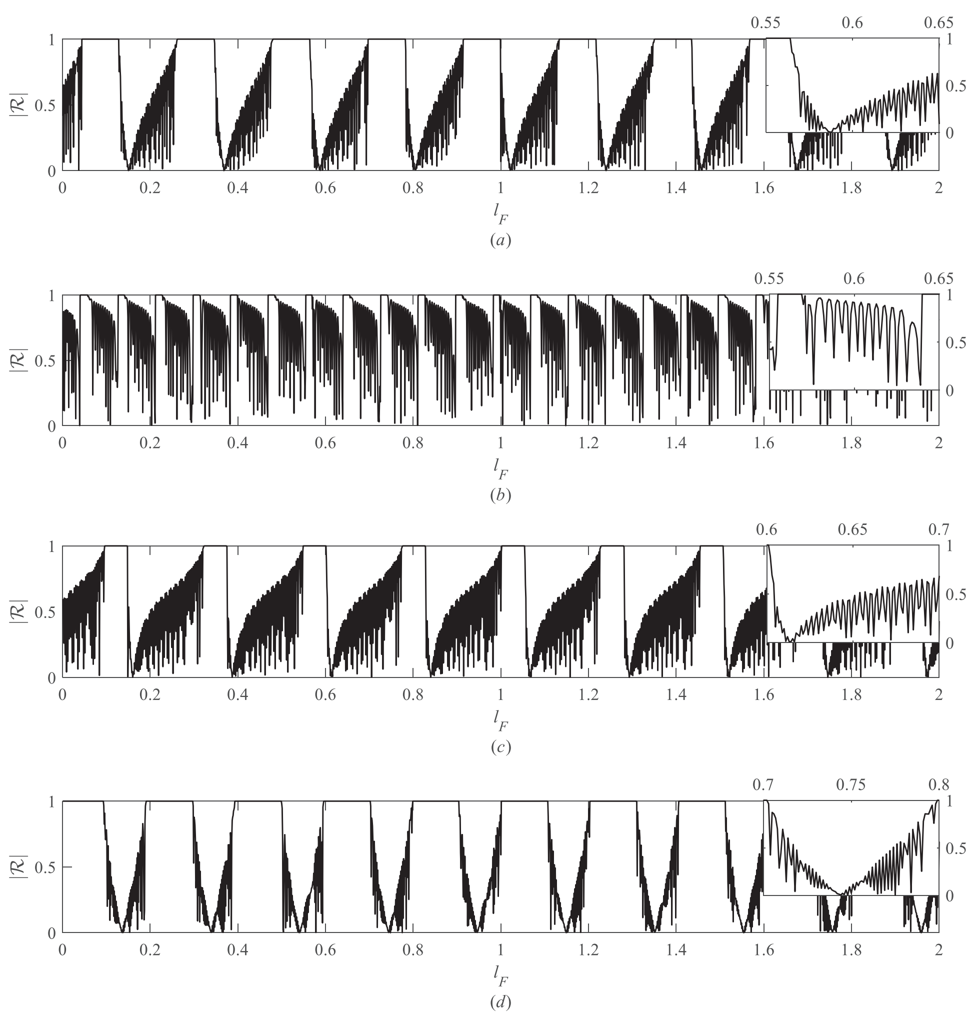

FIG. 14. The modulus of reflection coefficient $\mathcal{R}$ against l_F. (a) $\sigma = 13.87$; (b) $\sigma = 14.43$; (c) $\sigma = 15.51$; (d) $\sigma = 36.7$ ($h_j = h = 0.01$, $m_j = m = 0.9$, $L_j = L = 45\,536$, $d_j = d = 0$, $l_{l,j} = l_l = 4.0$, $j = 1, \ldots, n$, $n = 65$).

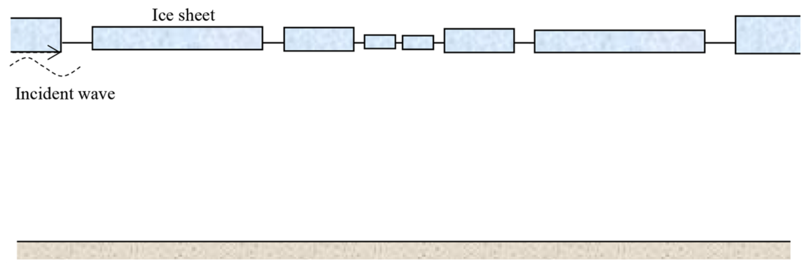

FIG. 15. Sketch of the problem.

case of $n = 65$. At low frequencies ($\sigma < 4$), $\left|\varepsilon^{(j)}\right|$ are close to 1, and $\left|\gamma^{(j)}\right|$ tend to 0, which is consistent with the results in Fig. 7, indicating that the majority of the waves are transmitted to the right hand side. At some discrete frequencies within the calculated range, $\left|\varepsilon^{(j)}\right|$ are equal to 1, $\left|\gamma^{(j)}\right| = 0$, which are also consistent with $|\mathcal{R}| = 0$ and $|\mathcal{T}| = 1$ in Fig. 7.

Figure 8 shows that at some frequencies, the magnitudes of $\left|\varepsilon^{(j)}\right|$ exceed 1 at $j = 32$, which does not imply that the overall reflection or transmission coefficient can be larger than one. Large $\left|\gamma^{(j)}\right|$ can also occur at $j = 31$. The peaks of $\left|\varepsilon^{(j)}\right|$ and $\left|\gamma^{(j)}\right|$ seem to appear at the same frequencies. At some of these frequencies, $\left|\varepsilon^{(j)}\right|$ and $\left|\gamma^{(j)}\right|$ are plotted, respectively, in Figs. 9 and 10, in particular, at $\sigma = 14.43$, 36.7, 13.87, and 15.51. Through these two figures, we may see that the coefficients are generally oscillatory with j. For $\sigma = 14.43$, only one peak occurs at $j = 32$ for $\left|\varepsilon^{(j)}\right|$ and at $j = 31$ for $\left|\gamma^{(j)}\right|$, or the value at the middle is much larger than those on the two sides. This seems to be similar to the behavior of an arrangement of vertical cylinders in the surface wave[30] and in the hydroelastic wave.[31]

Within the frequency span where $|\mathcal{R}|$ is close to one in Fig. 7, $\left|\varepsilon^{(j)}\right|$ in Fig. 8 are near the troughs of the curves and are lower than 1, and it is generally lower at larger j than that at smaller j. An example is shown in Fig. 11 at $\sigma = 16$. $\left|\varepsilon^{(j)}\right|$ and $\left|\gamma^{(j)}\right|$ tend to zero as j increases, leading the overall zero transmission to tend to zero.

C. The effect of ice sheet length

Further study is undertaken for the effect of the ice sheet length l_I at a given ice sheet number n and wave frequency σ. Figure 12 provides the results for the modulus of reflection and transmission coefficients at $n = 65$. It can be seen that at each σ, the results change periodically with l_I. In fact, the solution from the subdomain in Fig. 2 is independent of l_I. The solution of Eq. (22) will vary with S only. Noting that $S = e^{\kappa_0(l_F + l_I)}$ is a periodic function as κ_0 is a purely imaginary number, thus one can expect that the results will be periodic with respect to l_I. The exact period will be affected by σ. We may also notice that within each period the results oscillate rapidly with l_I. This is a typical behavior at large n. In Fig. 13, the same results of $\mathcal{R}$ for $n = 3$, $n = 5$, and $n = 9$ are plotted. It can be seen that the results are less oscillatory within a period at smaller n.

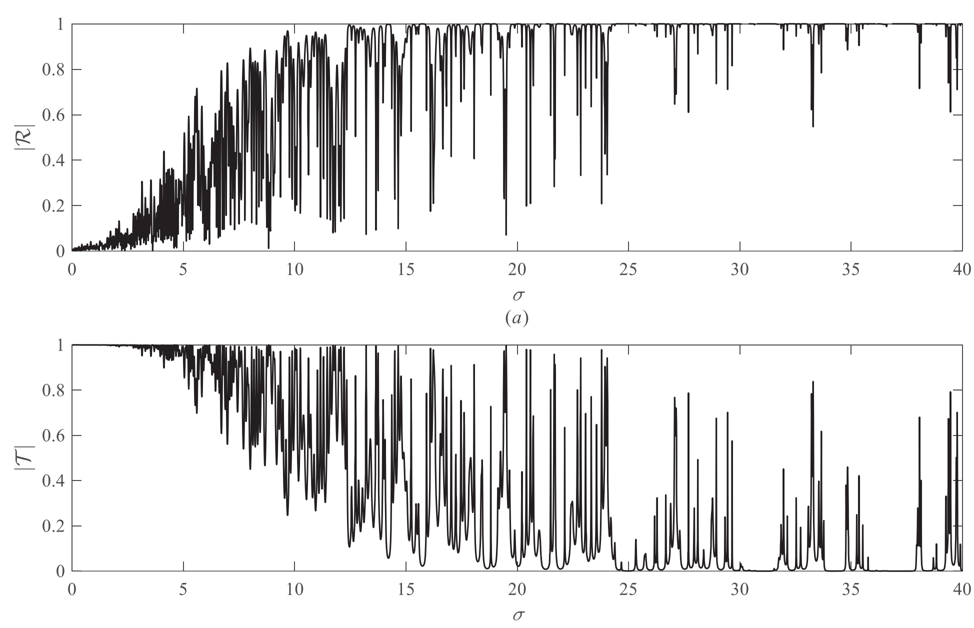

FIG. 16. The modulus of reflection $\mathcal{R}$ and transmission $\mathcal{T}$ coefficients of nonidentical subdomains. (a) $|\mathcal{R}|$ and (b) $|\mathcal{T}|$ ($h_1 = h_8 = 0.02$, $h_2 = h_3 = h_6 = h_7 = 0.01$, $h_4 = h_5 = 0.005$, $d_1 = d_8 = 0.018$, $d_2 = d_3 = d_6 = d_7 = 0.009$, $d_4 = d_5 = 0.0045$, $l_{F,1} = l_{F,7} = 2$, $l_{F,2} = l_{F,6} = 1$, $l_{F,3} = l_{F,5} = 0.5$, $l_{F,4} = 0.1$, $l_{I,2} = l_{I,7} = 16$, $l_{I,3} = l_{I,6} = 8$, $l_{I,4} = l_{I,5} = 4$, $H = 100$, $n = 8$).

It is interesting to see that the locations of the peaks are not affected by n.

D. The effect of the polynya width

Further simulations are carried out to investigate the effect of polynya width $l_{F,j} = l_F$. Figure 14 provides results for the reflection coefficients at $n = 65$. As in Fig. 12, the results are highly oscillatory. However, here the results from the subdomain in Fig. 2 will be different when l_F changes. Thus, R and T are also dependent on l_F at a given frequency or not exactly periodic. On the other hand, when l_F increases and is very large, the solution from the subdomain in Fig. 2 will tend to be periodic in terms of $e^{2\lambda_0 l_F}$.[28] In such a case, $\mathcal{R}$ in Fig. 14 will have two periodic components,

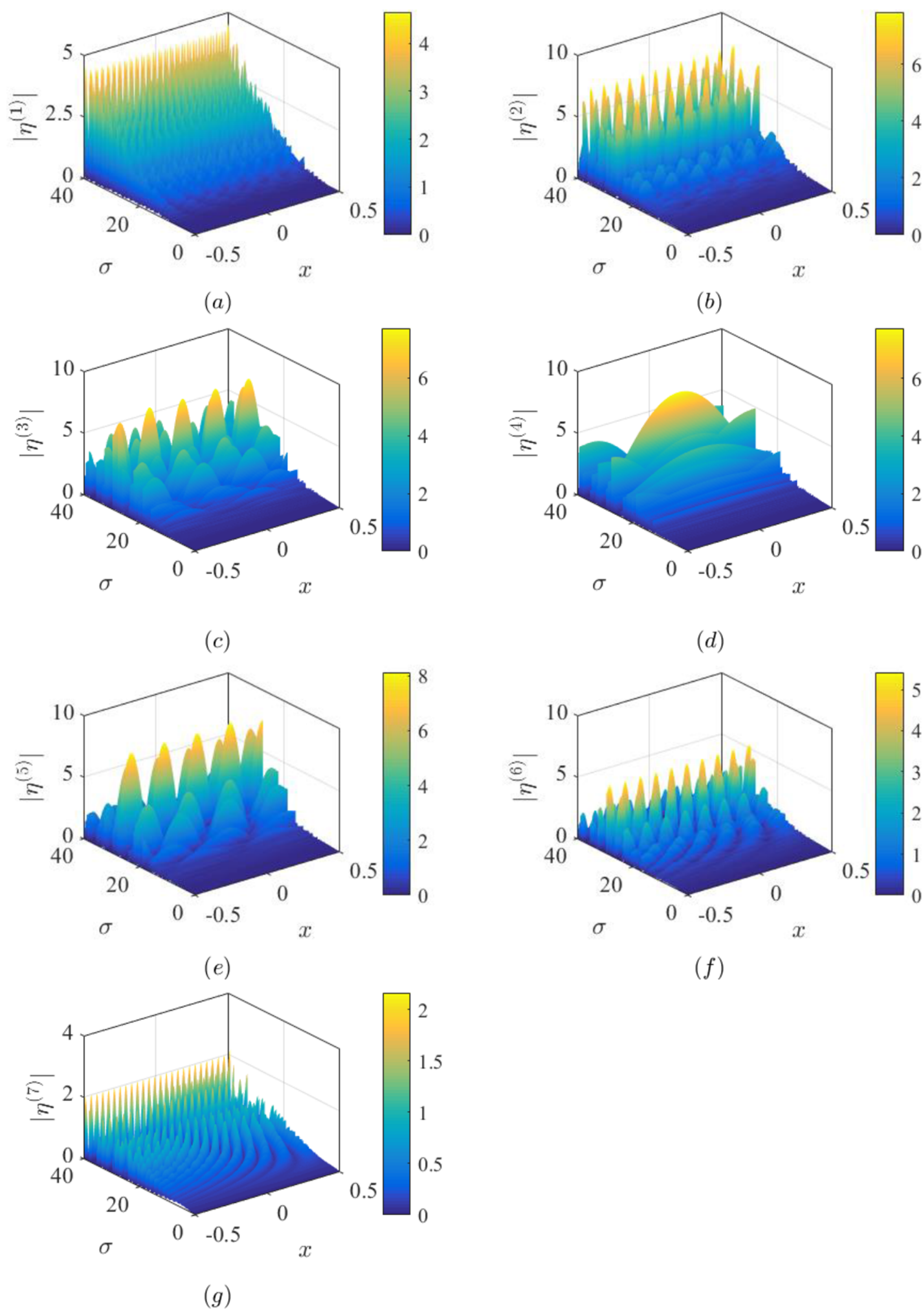

FIG. 17. Wave elevation in polynyas. (a) Ω_1; (b) Ω_2;(c) Ω_3; (d) Ω_4; (e) Ω_5; (f) Ω_6; (g) Ω_7($h_1 = h_8 = 0.02$, $h_2 = h_3 = h_6 = h_7 = 0.01$, $h_4 = h_5 = 0.005$, $d_1 = d_8 = 0.018$, $d_2 = d_3 = d_6 = d_7 = 0.009$, $d_4 = d_5 = 0.0045$, $l_{F,1} = l_{F,7} = 2$, $l_{F,2} = l_{F,6} = 1$, $l_{F,3} = l_{F,5} = 0.5$, $l_{F,4} = 0.1$, $l_{I,2} = l_{I,7} = 16$, $l_{I,3} = l_{I,6} = 8$, $l_{I,4} = l_{I,5} = 4$, $H = 100$, $n = 8$).

$e^{2\lambda_0 l_F}$ and $e^{2\kappa_0(l_F+l_I)}$, which makes its oscillatory behavior more complex.

E. Nonuniform polynya width and different ice sheets

We consider a case of nonuniform polynya width and different ice sheets to reflect more general practical problems. We set $n = 8$, $h_1 = h_8 = 0.02$,$h_2 = h_3 = h_6 = h_7 = 0.01$, $h_4 = h_5 = 0.005$. The ice draught is taken as $d_1 = d_8 = 0.018$,$d_2 = d_3 = d_6 = d_7 = 0.009$, $d_4 = d_5 = 0.0045$, and the length is taken as $l_{I,2} = l_{I,7} = 16$, $l_{I,3} = l_{I,6} = 8$, $l_{I,4} = l_{I,5} = 4$. The width of the subpolynya is $l_{F,1} = l_{F,7} = 2$, $l_{F,2} = l_{F,6} = 1$, $l_{F,3} = l_{F,5} = 0.5$, $l_{F,4} = 0.1$. A sketch of this nonuniform case is shown in Fig. 15.

The results are given in Fig. 16. As we can see, the reflection and transmission coefficients are very oscillatory with the dimensionless frequency. This is similar to the previous cases. However, the difference is that the pattern is highly irregular. Furthermore, unlike the identical subdomains, when the individual reflection coefficient of a subdomain is equal to zero, the overall $|\mathcal{R}|$ may not be zero due to the fact that the reflection coefficient in other polynyas may not be zero at this frequency. However, Fig. 16 shows that there are also a series of frequency spans within which $|\mathcal{R}| \to 1$ and $|\mathcal{T}| \to 0$ still occur, although the pattern is not regular.

The free surface wave elevation within each subpolynya is shown in Fig. 17. It can be seen that at each polynya, the surface wave has its own similar pattern. In fact, the surface wave at each polynya is principally based on the solution in the each subdomain shown in Fig. 2. The effects of other polynyas are through ε and γ. Therefore, these effects are on the amplitudes, not on the pattern itself. For this reason, because Ω_1 is the same as Ω_7, Ω_2 as Ω_6, and Ω_3 as Ω_5, their oscillatory wave patterns are similar.

IV. CONCLUSIONS

The solution for wave propagation through multiple polynyas has been presented. The procedure is based on a wide spacing approximation. By using the solutions of single polynyas and matching pressure and velocity at interfaces, a system of linear equations with unknown coefficients is established. The model and solution procedure has been verified though the comparison with results from the existing work. Extensive results are provided for the effect of the ice sheet number, ice sheet length, polynya width, and distribution of ice sheets, from which main conclusions can be drawn as follows:

(1) The wide spacing approximation model is accurate for wave propagation through multiple polynyas.
(2) For a multiple polynya with identical ice sheets, the reflection and transmission coefficients are more oscillatory with the wave frequencies when the number of ice sheets n is larger and local spikes can occur around the peaks and troughs.
(3) The overall reflection coefficients can be zero at series of discrete frequencies. For identical subdomains, or all individual polynyas being the same, it has been found that when there is no reflection at a single polynya, there will be no overall reflection. The overall transmission coefficient tends to zero at a series of frequency bands while n increases, which is similar to previously noted stopping band in the multicrack problem.
(4) For identical subpolynyas, at a given frequency, based on the wide spacing approximation, the reflection and transmission coefficients change periodically with the ice sheet length. They may not change periodically exactly with the polynya length. However, as the polynya width becomes large, the change follows two periodic components.
(5) For nonidentical polynyas, the distribution of ice sheet has a major effect on wave reflection and transmission. When there is no reflection in a single polynya, there may be still overall reflection.

ACKNOWLEDGMENTS

This work was supported by Lloyd's Register Foundation through the joint centre involving University College London, Shanghai Jiaotong University, and Harbin Engineering University, to which the authors are most grateful. Lloyd's Register Foundation helps protect life and property by supporting engineering-related education, public engagement, and the application of research. This work was also supported by the National Natural Science Foundation of China (Grant Nos. 51709131 and 51879123).

REFERENCES

[1] V. A. Squire, J. P. Dugan, P. Wadhams, P. J. Rottier, and A. K. Liu, "Of ocean waves and sea ice," Annu. Rev. Fluid Mech. **27**, 115 (1995).
[2] V. A. Squire, "Of ocean waves and sea-ice revisited," Cold Reg. Sci. Technol. **49**, 110 (2007).
[3] V. A. Squire, "Past, present and impendent hydroelastic challenges in the polar and subpolar seas," Philos. Trans. R. Soc., A **369**, 2813 (2011).
[4] G. Q. Robin, "Wave propagation through fields of pack ice," Philos. Trans. R. Soc., A **255**, 313 (1963).
[5] C. Fox and V. A. Squire, "Reflection and transmission characteristics at the edge of shore fast sea ice," J. Geophys. Res.: Oceans **95**, 11629, https://doi.org/10.1029/jc095ic07p11629 (1990).
[6] C. Fox and V. A. Squire, "Coupling between the ocean and an ice shelf," Ann. Glaciol. **15**, 101 (1991).
[7] C. Fox and V. A. Squire, "On the oblique reflexion and transmission of ocean waves at shore fast sea ice," Philos. Trans. R. Soc., A **347**, 185 (1994).
[8] T. Sahoo, T. L. Yip, and A. T. Chwang, "Scattering of surface waves by a semi-infinite floating elastic plate," Phys. Fluids **13**, 3215 (2001).
[9] M. H. Meylan and V. A. Squire, "The response of ice floes to ocean waves," J. Geophys. Res.: Atmos. **99**, 891, https://doi.org/10.1029/93jc02695 (1994).
[10] D. V. Evans and T. V. Davies, Wave-ice interaction Document No. 1313, 1968.
[11] H. Chung and C. Fox, "Calculation of wave-ice interaction using the Wiener-Hopf technique," N. Z. J. Math. **31**, 1 (2002).
[12] N. J. Balmforth and R. V. Craster, "Ocean waves and ice sheets," J. Fluid Mech. **395**, 89 (1999).
[13] L. A. Tkacheva, "Hydroelastic behavior of a floating plate in waves," J. Appl. Mech. Tech. Phys. **42**, 991 (2001).
[14] H. Chung and C. M. Linton, "Reflection and transmission of waves across a gap between two semi-infinite elastic plates on water," Q. J. Mech. Appl. Math. **58**, 1 (2005).
[15] T. D. Williams and V. A. Squire, "Scattering of flexural-gravity waves at the boundaries between three floating sheets with applications," J. Fluid Mech. **569**, 113 (2006).
[16] M. H. Meylan, L. G. Bennetts, C. Cavaliere, A. Alberello, and A. Toffoli, "Experimental and theoretical models of wave-induced flexure of a sea ice floe," Phys. Fluids **27**, 041704 (2015).
[17] M. D. Barrett and V. A. Squire, "Ice-coupled wave propagation across an abrupt change in ice rigidity, density, or thickness," J. Geophys. Res.: Oceans **101**, 20825, https://doi.org/10.1029/96jc01920 (1996).

[18] V. A. Squire and T. W. Dixon, "An analytic model for wave propagation across a crack in an ice sheet," Int. J. Offshore Polar Eng. **10**, 173 (2000).
[19] V. A. Squire and T. W. Dixon, "How a region of cracked sea ice affects ice-coupled wave propagation," Ann. Glaciol. **33**, 327 (2001).
[20] D. V. Evans and R. Porter, "Wave scattering by narrow cracks in ice sheets floating on water of finite depth," J. Fluid Mech. **484**, 143 (2003).
[21] R. Porter and D. V. Evans, "Scattering of flexural waves by multiple narrow cracks in ice sheets floating on water," Wave Motion **43**, 425 (2006).
[22] R. Porter and D. V. Evans, "Diffraction of flexural waves by finite straight cracks in an elastic sheet over water," J. Fluids Struct. **23**, 309 (2007).
[23] Z. F. Li, G. X. Wu, and C. Y. Ji, "Wave radiation and diffraction by a circular cylinder submerged below an ice sheet with a crack," J. Fluid Mech. **845**, 682 (2018).
[24] Z. F. Li, G. X. Wu, and Y. Y. Shi, "Wave diffraction by a circular crack in an ice sheet floating on water of finite depth," Phys. Fluids **30**, 117103 (2018).
[25] I. V. Sturova, "Radiation of waves by a cylinder submerged in water with ice floe or polynya," J. Fluid Mech. **784**, 373 (2015).
[26] K. Ren, G. X. Wu, and G. A. Thomas, "Wave excited motion of a body floating on water confined between two semi-infinite ice sheets," Phys. Fluids **28**, 127101 (2016).
[27] Z. F. Li, Y. Y. Shi, and G. X. Wu, "Interaction of waves with a body floating on polynya between two semi-infinite ice sheets," J. Fluids Struct. **78**, 86 (2018).
[28] Z. F. Li, Y. Y. Shi, and G. X. Wu, "Interaction of wave with a body floating on a wide polynya," Phys. Fluids **29**, 097104 (2017).
[29] Z. F. Li, G. X. Wu, and C. Y. Ji, "Interaction of wave with a body submerged below an ice sheet with multiple arbitrarily spaced cracks," Phys. Fluids **30**, 057107 (2018).
[30] H. D. Maniar and J. N. Newman, "Wave diffraction by a long array of cylinders," J. Fluid Mech. **339**, 309 (1997).
[31] K. Ren, G. Wu, and C. Ji, "Diffraction of hydroelastic waves by multiple vertical circular cylinders," J. Eng. Math. **113**, 45 (2018).